Immunity
Article

Cre-Mediated Cell Ablation Contests Mast Cell Contribution in Models of Antibody- and T Cell-Mediated Autoimmunity

Thorsten B. Feyerabend,[1,2,9] Anne Weiser,[1,2,9] Annette Tietz,[2] Michael Stassen,[5] Nicola Harris,[6] Manfred Kopf,[7] Peter Radermacher,[3] Peter Möller,[4] Christophe Benoist,[8] Diane Mathis,[8] Hans Jörg Fehling,[2] and Hans-Reimer Rodewald[1,2,*]

[1]Division for Cellular Immunology, Deutsches Krebsforschungszentrum (DKFZ), Im Neuenheimer Feld 280, 69120 Heidelberg, Germany
[2]Institute for Immunology
[3]Clinic for Anesthesiology
[4]Institute for Pathology
University of Ulm, 89081 Ulm, Germany
[5]Institute for Immunology, Johannes Gutenberg-Universität, Langenbeckstr. 1, 55131 Mainz, Germany
[6]Swiss Vaccine Research Institute and Global Health Institute, Ecole Polytechnique Fédérale de Lausanne (EPFL), 1015 Lausanne, Switzerland
[7]ETH Zürich, Institute for Integrative Biology Wagistrasse 27, 8952 Zürich-Schlieren, Switzerland
[8]Department of Pathology, Harvard Medical School, Boston, MA 02115, USA
[9]These authors contributed equally to this work
*Correspondence: hr.rodewald@dkfz.de
DOI 10.1016/j.immuni.2011.09.015

SUMMARY

Immunological functions of mast cells remain poorly understood. Studies in *Kit* mutant mice suggest key roles for mast cells in certain antibody- and T cell-mediated autoimmune diseases. However, *Kit* mutations affect multiple cell types of both immune and nonimmune origin. Here, we show that targeted insertion of Cre-recombinase into the mast cell carboxypeptidase A3 locus deleted mast cells in connective and mucosal tissues by a genotoxic Trp53-dependent mechanism. Cre-mediated mast cell eradication (Cre-Master) mice had, with the exception of a lack of mast cells and reduced basophils, a normal immune system. Cre-Master mice were refractory to IgE-mediated anaphylaxis, and this defect was rescued by mast cell reconstitution. This mast cell-deficient strain was fully susceptible to antibody-induced autoimmune arthritis and to experimental autoimmune encephalomyelitis. Differences comparing *Kit* mutant mast cell deficiency models to selectively mast cell-deficient mice call for a systematic re-evaluation of immunological functions of mast cells beyond allergy.

INTRODUCTION

Whereas the central role of IgE, high-affinity Fc receptors (FcR) for IgE (FcεRI), and mast cells in IgE-mediated allergic diseases is evident, other pathological or protective immunological functions of mast cells remain enigmatic. Insight into in vivo mast cell functions relies primarily on animals lacking mast cells. Mutations in the gene encoding the receptor tyrosine kinase Kit are referred to as white-spotted (*W*) *Kit* alleles and cause mast cell deficiency. Hypomorphic Kit^{W/W^v} (Kitamura et al., 1978) and, more recently, $Kit^{W\text{-}sh/W\text{-}sh}$ (Berrozpe et al., 1999; Grimbaldeston et al., 2005) mutants have served as standard models to study mast cell functions. However, Kit signaling is not only important for mast cell development but also affects many other lineages, including hematopoietic stem and progenitor cells, red blood cells, neutrophils, intestinal pacemaker cells, melanocytes, and germ cells. Also, Kit is involved in the regulation of pain and metabolic responses (reviewed in Besmer et al., 1993; Broudy, 1997; Di Santo and Rodewald, 1998; Fleischman, 1993; Galli et al., 1994). Because pleiotropic Kit functions have hampered an unequivocal assignment of a given phenotype specifically to the lack of mast cells, strategies have been developed to selectively reconstitute *Kit* mutants with bone marrow-derived cultured mast cells (BMMC) (Nakano et al., 1985). In this approach, nonreconstituted *Kit* mutants are compared to BMMC-reconstituted *Kit* mutants in any given assay (Tsai et al., 2005). By and large, this system is the foundation of the current concept of mast cells as key immunological elements involved in an increasing list of physiological and pathological functions. These encompass not only roles for mast cells in positive or negative regulation of innate and adaptive immune responses (reviewed in de Vries and Noelle, 2010; Galli et al., 2008) and in defense against bacterial infections (reviewed in Abraham and St John, 2010) and toxins (Metz et al., 2006; Schneider et al., 2007) but also invoke mast cell contributions to autoimmunity (Benoist and Mathis, 2002; Sayed et al., 2008), obesity and diabetes (Liu et al., 2009), arteriosclerosis (Kovanen, 2009), and cancer (Tlsty and Coussens, 2006). Given the underlying *Kit* deficiency, it remains ambiguous to what extent the absence of mast cells is, in fact, responsible for the observed phenotypes. It is also noteworthy that in *Kit* mutants mast cell deficiency cannot readily be combined with key

immunological factors such as major histocompatibility complex (MHC) haplotypes, genetic backgrounds, or informative immunological mutations. The mast cell deficiency is largely limited in $Kit^{W/Wv}$ mice to the WB × C57BL/6 genetic background (for origin of MHC in this strain see Waskow et al., 2009) and for $Kit^{W\text{-}sh/W\text{-}sh}$ mice predominantly, but not completely (Lu et al., 2006), to the C57BL/6 genetic background (Grimbaldeston et al., 2005). Taken together, mouse strains wild-type for *Kit*, but selectively deficient for mast cells, and on defined genetic backgrounds would be advantageous.

We show here that expression of Cre recombinase from the *mast cell carboxypeptidase A* (*Cpa3*) locus (Feyerabend et al., 2009) selectively abrogated mast cells in vivo. The mast cell deficiency in "Cre-mediated mast cell eradication" (Cre-Master) mice was Kit independent and constitutive. We subjected Cre-Master mice to passive autoantibody-driven arthritis and active immunization-driven experimental autoimmune encephalomyelitis (EAE), i.e., models of autoimmunity in which major propathogenic roles for mast cells had been reported in Kit mutants (Lee et al., 2002; Secor et al., 2000; reviewed in Sayed et al., 2008). We found no evidence for an involvement of mast cells in these two models of autoimmune diseases, thus providing examples in which analyses of mast cells in *Kit* mutant mice may not reflect mast cell functions in a normal immune system.

RESULTS

Ablation of Connective Tissue Mast Cells by Expression of Cre Recombinase from the *Carboxypeptidase A* Locus

The *Cpa3* gene, which encodes the mast cell protease carboxypeptidase A (Cpa3), is considered a mast cell-specific gene (Reynolds et al., 1989) that is expressed from the earliest mast cell progenitors on (Rodewald et al., 1996). To drive Cre expression in the mast cell lineage, we generated mice in which improved Cre recombinase (iCre), mutated according to mammalian codon usage (Shimshek et al., 2002), was inserted via homologous recombination into the *Cpa3* locus, which yielded the $Cpa3^{Cre}$ allele (Figure S1 available online; Feyerabend et al., 2009). Rather than finding Cre expression in mast cells, we noted a complete absence of mast cells in the peritoneal cavity from heterozygous $Cpa3^{Cre/+}$ gene-targeted mice (Figures 1A and 1B). Lack of mast cells was evident by flow cytometric comparison of peritoneal lavage cells from $Cpa3^{+/+}$ and $Cpa3^{Cre/+}$ mice for the mast cell phenotype $Kit^+Fc\varepsilon RI^+$ (Figures 1A and 1B; quantified in 1E). To test whether mast cells were morphologically present but lacked expression of Kit and FcεRI, cytospins from peritoneal lavage cells were examined for mast cell-typical metachromatic May-Grünwald-Giemsa staining (Figures 1A and 1B). Again, mast cells were undetectable in $Cpa3^{Cre/+}$ mice. We extended these findings to the skin, another prominent anatomical location for connective tissue mast cells (CTMC). Ears from $Cpa3^{+/+}$ and $Cpa3^{Cre/+}$ mice were stained by toluidine blue and by chloroacetate esterase, and dye-reactive cells were found in skin from wild-type but not $Cpa3^{Cre/+}$ mice (Figures 1C and 1D).

Next, we comprehensively searched for a mast cell gene expression signature in normally mast cell-bearing tissues. Total mRNAs from peritoneal lavage cells (Figure 1F) and skin (Figure 1G) of $Cpa3^{+/+}$, $Cpa3^{Cre/+}$, and $Kit^{W/Wv}$ mice were subjected to whole-genome gene expression analyses. Consistent with their specific expression in CTMC, the protease genes *Cma2*, *Cpa3*, *Mcpt4*, *Mcpt5*, and *Mcpt6* were strongly represented among peritoneal lavage- and skin-derived mRNAs from wild-type mice. Of note, none of these mast cell-specific transcripts was detectable in $Cpa3^{Cre/+}$ or in $Kit^{W/Wv}$ mRNAs (Figures 1F and 1G). As expected from connective tissues, mucosal mast cell- or basophil-associated proteases (*Mcpt1, Mcpt2, Mcpt8, Mcpt9*) were not expressed in peritoneal cells and skin in any of the strains. In further support of the lack of mast cell products, expression of *Fcer1a* and *Kit* was undetectable in the peritoneal cavity of $Cpa3^{Cre/+}$ and $Kit^{W/Wv}$ mice. In the skin, Kit-expressing cells include mast cells and melanocytes (Aoki et al., 2009; Peters et al., 2002). Consistent with the lack of mast cells but not melanocytes, *Kit* expression was reduced in $Cpa3^{Cre/+}$ skin. The source of this remaining *Kit* expression was nonhematopoietic because Kit^+CD45^+ cells were undetectable by flow cytometry in the skin of $Cpa3^{Cre/+}$ mice. Kit^+ cells, which were detected by immunhistology in the skin of $Cpa3^{Cre/+}$ mice, lacked mast cell gene expression and were exclusively localized in close vicinity to hair follicles (not shown). This is consistent with the characteristics of melanocyte lineage cells. In $Kit^{W/Wv}$ skin, lack of melanocytes, evident by absence of melanocyte-specific gene (*Si* and *Dct*) expression, and mast cells abrogated *Kit* expression. *Gata2*, a transcription factor important for mast cell development, and histidin decarboxylase (*Hdc*), which is expressed in mast cells and monocytes, were similarly reduced in $Cpa3^{Cre/+}$ and $Kit^{W/Wv}$ compared to wild-type mice. Collectively, the complete loss of mast cell products in tissues that are normally rich in mast cells supports the conclusion that $Cpa3^{Cre/+}$ mice are fully mast cell deficient. A direct comparison of mast cell signatures in $Cpa3^{Cre/+}$ and $Kit^{W/Wv}$ mice demonstrates that the extent of mast cell deficiency was indistinguishable in both strains. Analysis for gene expression of Fc receptors, interleukins (Il) *Il4*, *Il6*, *Il9*, *Il10*, as well as *Tnf* and *Ifng* in the peritoneal cavity and in skin (Figures 1F and 1G), and of chemokines, chemokine receptors, and adhesion molecules in spleens (not shown) revealed no effect of Cre-mediated mast cell ablation on these parameters.

Skin mast cell numbers can be markedly increased by chronic inflammation. After repeated exposure of skin over 6 weeks to phorbol-12-myristate-13-acetate (PMA), mast cell numbers increased 3- to 4-fold in wild-type mice. The relative increase in mast cell numbers was even higher (10- to 100-fold) in the skin of normally mast cell-deficient $Kit^{W/Wv}$ mice (Figure 1H; Gordon and Galli, 1990; Waskow et al., 2007). Hence, inflammatory signals can partially overcome the block in mast cell development in $Kit^{W/Wv}$ mice. In contrast, the skin of $Cpa3^{Cre/+}$ mice remained free of mast cells when challenged by chronic skin inflammation (Figure 1I). Taken together, $Cpa3^{Cre/+}$ mice showed a complete and constitutive absence of mast cells in peritoneal cavity and in skin, which was accompanied by the loss of a mast cell gene expression signature. Even under conditions of chronic skin inflammation, no mast cells were induced in $Cpa3^{Cre/+}$ mice.

$Cpa3^{Cre/+}$ Mice Lack Mucosal Mast Cells in the Intestine

At mucosal sites, mast cells are very rare unless induced by infection or inflammation. To generate intestinal mastocytosis,

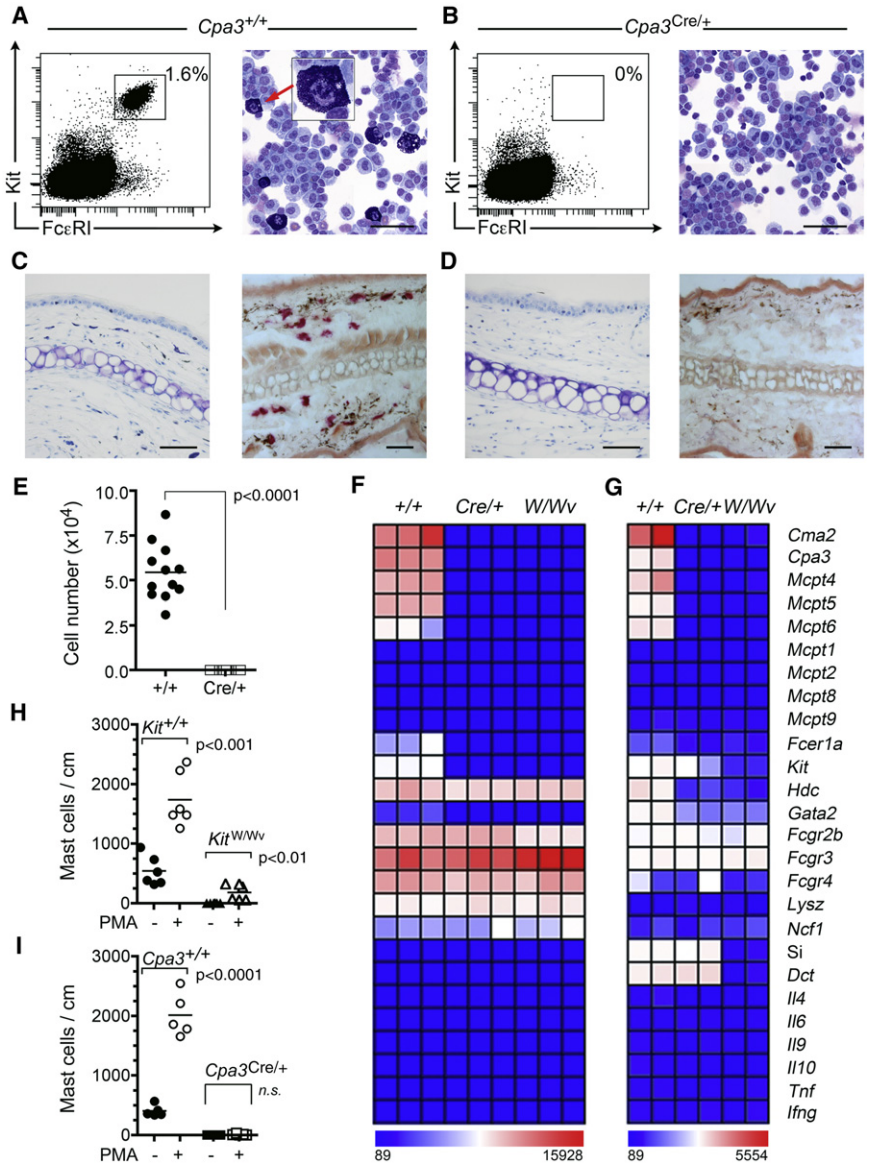

Figure 1. *Cpa3*$^{Cre/+}$ Mice Lack Mast Cells in the Peritoneal Cavity and the Skin

(A and B) Peritoneal lavage cells from *Cpa3*$^{+/+}$ (A, left) and *Cpa3*$^{Cre/+}$ (B, left) mice were analyzed by flow cytometry without prior forward and side scatter gating for the presence of Kit^{+}FcεRI^{+} mast cells (gated regions in A and B). Expression of FcεRI was revealed by anti-IgE staining. Numbers show percentages of mast cells in total peritoneal lavage cells. Cytospins from peritoneal lavage cells from *Cpa3*$^{+/+}$ (A, right) and *Cpa3*$^{Cre/+}$ (B, right) mice were analyzed by May-Grünwald-Giemsa staining for metachromatic mast cells. The insert (A, right) shows a 3× magnification of the neighboring mast cell (arrow). Details on the generation of the *Cpa3*^{Cre} allele are given in Figure S1.

(C and D) Ear skin sections from *Cpa3*$^{+/+}$ (C) and *Cpa3*$^{Cre/+}$ (D) mice were analyzed by toluidine blue for metachromatic mast cells (left) and by chloroacetate esterase for purple-stained mast cells (right).

Scale bars represent 50 μm.

(E) Quantification of absolute numbers of mast cells in the peritoneal cavity of *Cpa3*$^{+/+}$ (closed circle) (54,000 ± 1,500 [one standard deviation]; n = 12 mice) and *Cpa3*$^{Cre/+}$ (open square) (0.0 ± 0.0; n = 12) mice. Numbers were determined by flow cytometry. Each symbol represents an individual mouse.

(F and G) Mast cell gene expression signature in peritoneal lavage cells (F) and in ears (G). Total mRNAs from peritoneal lavage cells were analyzed by global gene expression arrays. The genes listed on the right were compared between *Cpa3*$^{+/+}$, *Cpa3*$^{Cre/+}$, and *Kit*$^{W/Wv}$ mice (each n = 3). (G) Total mRNAs from ears were analyzed as in (F) and compared between *Cpa3*$^{+/+}$, *Cpa3*$^{Cre/+}$, and *Kit*$^{W/Wv}$ mice (each n = 2). The heat maps in (F) and (G) are globally normalized for all genes shown in each panel, and the color code (bottom) shows the corresponding differences in gene expression.

(H and I) Mast cell numbers after repeated exposure of skin over 6 weeks to phorbol-12-myristate-13-acetate (PMA). In (H), untreated (closed circle) (540 ± 247 mast cells per cm ear skin, n = 6) and PMA-treated (open circle) (1,734 ± 454, n = 6) *Kit*$^{+/+}$ mice were compared to untreated (closed triangle) (1.3 ± 0.8, n = 6) and PMA-treated (open triangle) (179 ± 136, n = 6) *Kit*$^{W/Wv}$ mice. In (I), untreated (closed circle) (404 ± 95, n = 5) and PMA-treated (open circle) (2,008 ± 363, n = 5) *Cpa3*$^{+/+}$ mice were compared to untreated (closed square) (0.2 ± 0.3, n = 5) and PMA-treated (open square) (10 ± 12.8, n = 5) *Cpa3*$^{Cre/+}$ mice. Numbers were determined histologically by toluidine blue staining, and each symbol represents an individual mouse.

we infected mice with the prototypic T helper 2 (Th2) cell-inducing helminth *Nippostrongylus brasiliensis* (*Nb*). Mast cells resident in the lamina propria and epithelium of the small intestine in helminth-infected mice selectively express mast cell protease 1 (Mcpt1), a mucosal mast cell (MMC)-specific marker (Friend et al., 1996). In a first set of experiments, small intestines were taken 10 days after the infection, and histological sections were analyzed by toluidine blue staining. Although numerous MMCs were induced in the mucosa of *Cpa3*$^{+/+}$ mice (Figure 2A), MMCs remained undetectable in *Cpa3*$^{Cre/+}$ mice (Figure 2B). In a second set of experiments, we evaluated the mucosal mast cell response based on local and systemic Mcpt1 expression. In noninfected mice, *Mcpt1* mRNA was found at very low amounts and Mcpt1 protein was undetectable. At 14 days after the infection, abundant quantities of *Mcpt1* mRNA and Mcpt1 protein were induced only in *Cpa3*$^{+/+}$ mice. In *Cpa3*$^{Cre/+}$ mice, *Mcpt1* mRNA expression did not increase compared to noninfected mice, and Mcpt1 protein remained undetectable (Figures 2C and 2D). In further characterization of *Mcpt1* mRNA-expressing cells in *Cpa3*$^{Cre/+}$ mice, we quantified by flow cytometry the percentage and the absolute number of mast cell progenitors (MCPs) (Arinobu et al., 2005). The results show that MCPs were barely detectable in *Cpa3*$^{Cre/+}$ (absolute number of cells = 1.68 ± 0.49 × 10^2; n = 4) compared to *Cpa3*$^{+/+}$ (11.7 ± 6.18 × 10^2; n = 4) mice (Figure S2). RT-PCR analysis of sorted cells for *Mcpt1* mRNA identified the few MCPs as a likely source of

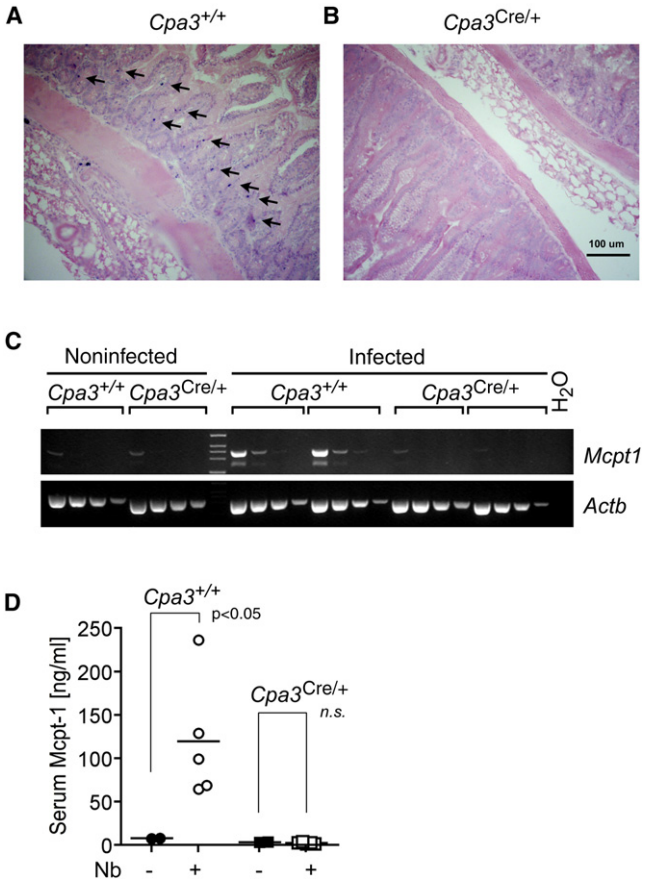

Figure 2. *Cpa3*$^{Cre/+}$ Mice Lack Mucosal Tissue Mast Cells

(A and B) *Cpa3*$^{+/+}$ and *Cpa3*$^{Cre/+}$ mice were infected with the helminth *Nippostrongylus brasiliensis*. The small intestine was taken 10 days post-infection, and sections from the jejunum from *Cpa3*$^{+/+}$ (n = 3) (A) and *Cpa3*$^{Cre/+}$ (n = 3) (B) mice were analyzed for mucosal mast cells by toluidine blue staining. Arrows point at mast cells in the mucosa in *Cpa3*$^{+/+}$ mice that were absent in *Cpa3*$^{Cre/+}$ mice.

(C and D) Intestinal mRNA (C) and serum (D) samples, taken 14 days post-infection from *Cpa3*$^{+/+}$ (n = 5) and *Cpa3*$^{Cre/+}$ (n = 5) mice and from noninfected mice (n = 2 for each genotype), were analyzed for expression of Mcpt1. In (C), *Mcpt1* mRNA expression was analyzed by RT-PCR on mice of the indicated genotype with and without infection. For relative comparison, cDNAs were diluted in 10-fold steps, and templates were normalized for *Actb* mRNA expression (see also Figure S2). In (D), serum concentrations of Mcpt1 were determined by ELISA, and results are shown for uninfected (closed circle) and infected (open circle) *Cpa3*$^{+/+}$ mice and for uninfected (closed square) and infected (open square) *Cpa3*$^{Cre/+}$ mice. Each symbol represents an individual mouse.

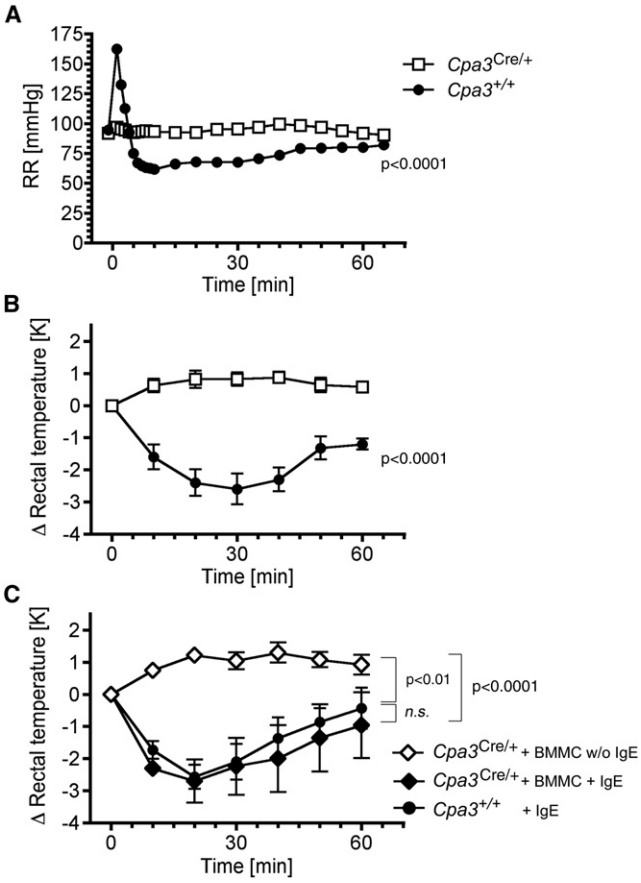

Figure 3. Lack of Anaphylaxis in *Cpa3*$^{Cre/+}$ Mice and Rescue of the Defect by Mast Cell Transplantation

(A–C) *Cpa3*$^{Cre/+}$ and control mice were analyzed by systemic passive anaphylaxis. Data on local (cutaneous) anaphylaxis are shown in Figure S3.

(A) Systolic blood pressure in anesthetized *Cpa3*$^{+/+}$ (closed circle) and *Cpa3*$^{Cre/+}$ (open square) mice was recorded in the carotid artery after sensitization by intravenous injection of anti-DNP IgE and challenge on the next day by intravenous injection with DNP-human serum albumin. *Cpa3*$^{+/+}$ and *Cpa3*$^{Cre/+}$ mice were analyzed pair-wise on the same day. Data shown are representative for one out of two experiments with one mouse per genotype in each experiment.

(B) Rectal temperatures of *Cpa3*$^{+/+}$ (closed circle) and *Cpa3*$^{Cre/+}$ (open square) were recorded in 10 min intervals and are expressed as temperature difference (Δ) compared to starting temperature. Mice were sensitized as in (A) and challenged on the subsequent day by intravenous injection with DNP-Ovalbumin. Shown are the mean ± SEM for five mice per genotype.

(C) Mast cell transplantation rescues anaphylaxis in *Cpa3*$^{Cre/+}$ mice. BMMC-transplanted *Cpa3*$^{Cre/+}$ mice were challenged as described in (B), and the temperature drop was recorded (closed diamond) (n = 5). Negative control *Cpa3*$^{Cre/+}$ mice also received mast cells, but IgE was omitted prior to antigen challenge (open diamond) (n = 5). As positive controls, *Cpa3*$^{+/+}$ mice were included and treated as described in (C) (closed circle) (n = 3). In all mice, rectal temperatures were recorded in 10 min intervals and are expressed as temperature difference (Δ) compared to starting temperature. Shown are the mean ± SEM.

Mcpt1 expression in noninfected mice (Figure S2). Because MCPs express *Mcpt1* mRNA and *Mcpt1* marker expression was not induced in response to *Nb* infection in *Cpa3*$^{Cre/+}$ mice, it is very unlikely that MCPs participate in this inflammatory response. Altogether, *Cpa3*$^{Cre/+}$ mice were unable to generate a mucosal mast cell response to *Nb* infection.

Cpa3$^{Cre/+}$ Mice Are Refractory to IgE-Driven Anaphylactic Responses

To functionally test for the absence of mast cells, we subjected mice to IgE-mediated local and systemic anaphylactic responses (Figure 3; Figure S3). Mice were injected intradermally into the ear or intravenously with anti-dinitrophenyl (DNP) IgE monoclonal antibody, followed on the next day by systemic challenge with hapten (DNP)-carrier antigens with (local) or without (systemic) Evans blue as an extravasation tracer. For better

visualization, passive cutaneous anaphylaxis was done in *Cpa3*$^{+/+}$ and *Cpa3*$^{Cre/+}$ mice on the white BALB/c background. In IgE- but not in PBS control-injected ears, Evans blue extravasated within 5 min into the tissue. In *Cpa3*$^{Cre/+}$ mice, IgE-injected ears remained white (Figure S3).

Systemic IgE-mediated anaphylactic responses were measured by changes in systolic blood pressure and in body temperature. Systolic blood pressure was read in anesthesia after catheterization of the carotid artery (Albuszies et al., 2005) in mice loaded with IgE on the previous day. After intravenous antigen challenge, the mean blood pressure rose from ~95 mm Hg to ~170 mm Hg within 2 min, followed by a sudden and massive drop to ~60 mm Hg, from where it slowly recovered (Figure 3A). This blood pressure response coincided with a marked increase in heart rate from ~400 to >550 beats per min, which also returned to the baseline over time. This hemodynamic response pattern is typical for a nonlethal anaphylactic shock. In *Cpa3*$^{Cre/+}$ mice, blood pressure (Figure 3A) and heart rate remained unaffected by the antigen challenge. When body temperature was read as a measure for systemic anaphylaxis under nonlethal conditions, *Cpa3*$^{+/+}$ mice showed a severe transient drop in body temperature whereas *Cpa3*$^{Cre/+}$ mice did not respond (Figure 3B). To examine whether mast cells would restore anaphylactic responsiveness, *Cpa3*$^{Cre/+}$ mice were transplanted with cultured mast cells. Mast cell-reconstituted *Cpa3*$^{Cre/+}$ mice mounted a normal anaphylactic temperature drop that was comparable to that of wild-type mice (Figure 3C). Collectively, *Cpa3*$^{Cre/+}$ mice were resistant to IgE-mediated anaphylaxis, and this deficiency could be rescued by mast cell transplantation.

Genotoxicity and Trp53 Dependency of *Cpa3*^{Cre}-Driven Mast Cell Ablation

Cre-mediated cell ablation was cell intrinsic to the hematopoietic system because wild-type bone marrow stem cells reconstituted donor mast cells in irradiated *Cpa3*$^{Cre/+}$ recipients, and *Cpa3*$^{Cre/+}$ bone marrow stem cells were unable to reconstitute mast cells in *Kit*$^{W/Wv}$ mice (Figure S4). Loss of mast cells in *Cpa3*$^{Cre/+}$ gene-targeted mice was not due to the heterozygous disruption of the *Cpa3* gene because even homozygous *Cpa3*$^{-/-}$ gene-deficient mice have normal numbers of mast cells (Feyerabend et al., 2005). Southern blotting showed that the targeting construct had inserted correctly into the *Cpa3* locus (Figure S1), whereas no other gene has been disrupted in this strain.

Cpa3 is very strongly expressed in mast cells (discussed further below). In cell lines and in mice, strong or prolonged expression of Cre has been reported to exert genotoxicity via cutting of "endogenous loxP-like sites" in the mouse genome (Naiche and Papaioannou, 2007; Schmidt-Supprian and Rajewsky, 2007), and Cre-induced genotoxicity can result in chromosomal abnormalities (Higashi et al., 2009). To search for such signs of Cre toxicity, we derived bone marrow mast cells (BMMCs) from *Cpa3*$^{Cre/+}$ mice. Despite the fact that *Cpa3*$^{Cre/+}$ bone marrow was extremely inefficient in generating mast cells in vitro compared to wild-type bone marrow (Figure S4), the resulting cells provided sufficient material for further characterization. In contrast to wild-type BMMCs that had a normal karyotype, chromosome spreads from *Cpa3*$^{Cre/+}$ BMMCs included a fusion chromosome (Figure S4). To identify the chromosome that contributed to this pseudotrisomy and to identify further gains or losses, we subjected genomic DNA from *Cpa3*$^{Cre/+}$ BMMCs to array-based comparative genomic hybridization (aCGH). This higher-resolution technique revealed a large deletion on chromosome 7 and two small deletions on chromosomes 7 and 11 in this preparation. The major part of chromosome 16 was duplicated, consistent with the large fusion chromosome visualized by the chromosome spreads (Figure S4). Such genomic lesions are compatible with a genotoxic mechanism of mast cell ablation.

We hypothesized that p53 (*Trp53*)-dependent DNA repair and apoptosis pathways (reviewed in Vousden and Lane, 2007) might be activated in *Cpa3*$^{Cre/+}$ mast cells in response to Cre-induced DNA double-strand breaks and that repeated DNA lesions might drive mast cells into apoptosis. To test this possibility, we crossed *Cpa3*$^{Cre/+}$ mice onto a *Trp53*$^{-/-}$ background. As expected, mast cells were present in control (*Cpa3*$^{+/+}$*Trp53*$^{+/+}$ and *Cpa3*$^{+/+}$*Trp53*$^{-/-}$) but not in *Cpa3*$^{Cre/+}$*Trp53*$^{+/+}$ mice. Interestingly, peritoneal mast cells were partially rescued in *Cpa3*$^{Cre/+}$ on a *Trp53*$^{-/-}$ background (Figure 4A). Consistent with Cre-induced genomic lesions, rescued peritoneal mast cells, but not wild-type mast cells, showed multinucleated or fragmented nuclei (Figure 4B). Loss of Trp53 in *Cpa3*$^{Cre/+}$ mice also rescued mast cells in the skin (Figure 4C). The fact that this rescue was only partial in terms of cells per mouse and numbers of mice with mast cells (Figure 4D) suggests that rescued mast cells were highly unstable even when the Trp53 pathway was blocked.

Collectively, the data imply that strong expression of Cre recombinase causes DNA breaks in mast cells, evident by genomic imbalances, and that mast cell ablation occurs by a Trp53-dependent mechanism.

Hematological and Immunological Parameters and Th2 Cell-Dependent Antibody Response in the Absence of Mast Cells

To establish key immunological and hematological parameters, we determined in the peripheral blood of *Cpa3*$^{+/+}$ and *Cpa3*$^{Cre/+}$ mice (C57BL/6 background) counts of total white blood cells, red blood cells, platelets, hematocrit, and percentages of lymphocytes, monocytes, and neutrophils. None of these parameters differed between normal and mast cell-deficient mice (Figure 5A). Spleens were analyzed for immature and mature B cell populations, for naive, activated, and memory CD4$^+$ and CD8$^+$ T cells, and for neutrophils, macrophages, and dendritic cell populations (Figure S5). None of these populations was affected by the absence of mast cells. The only cell type other than mast cells that was affected in *Cpa3*$^{Cre/+}$ mice were splenic basophils ($1.62 \pm 0.61 \times 10^5$ in *Cpa3*$^{+/+}$ mice versus $0.63 \pm 0.21 \times 10^5$ in *Cpa3*$^{Cre/+}$ mice; n = 12 for each genotype). Basophils were also reduced in *Kit*$^{W/Wv}$ spleens ($0.18 \pm 0.05 \times 10^5$ basophils per spleen; n = 7) (Figure S5), which is in agreement with the reported reduction of basophils in *Kit*$^{W/Wv}$ blood (Mancardi et al., 2011). Finally, no differences were observed for IgM, IgG1, IgG2a, IgG2b, IgG3, IgA, and IgE serum titers comparing nonimmunized *Cpa3*$^{+/+}$ and *Cpa3*$^{Cre/+}$ mice (Figure 5B), which implies that IgE titers are regulated independently of IgE adsorption by FcεRI-bearing mast cells.

To elicit a Th cell-dependent antibody response predominated by IL-4-mediated IgG1 class switch, mice were immunized with

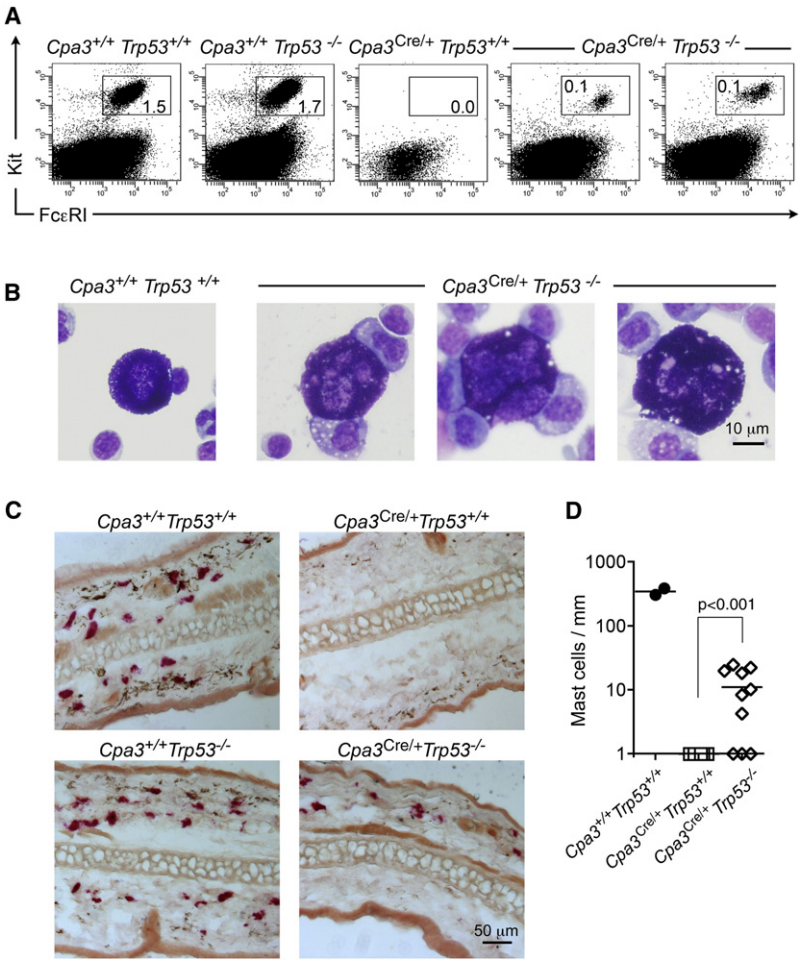

Figure 4. Mechanism of Cre Recombinase-Mediated Ablation of Mast Cells

(A) Peritoneal lavage cells from mice of the indicated genotypes were analyzed by flow cytometry for the presence of Kit$^+$FcεRI$^+$ mast cells. Two examples are provided for *Cpa3*$^{Cre/+}$*Trp53*$^{-/-}$ mice. Numbers in the gates show percentages of mast cells in total peritoneal lavage cells.

(B) May-Grünwald-Giemsa-stained cytospins of peritoneal lavage cells of the indicated genotypes, showing multinucleated or fragmented nuclei in rescued mast cells from *Cpa3*$^{Cre/+}$*Trp53*$^{-/-}$ mice. Further information on the mechanism of mast cell ablation is given in Figure S4.

(C) Histological analysis of ear skin mast cells of the indicated genotypes by chloroacetate esterase staining.

(D) Quantification of mast cells in the ears of *Cpa3*$^{Cre/+}$ *Trp53*$^{-/-}$ mice. Mast cells were counted on chloroacetate esterase-stained sections as in (C). Each symbol represents an individual mouse.

NP-chicken gamma globulin (NP-CGG) in alum. At 14 days post-immunization, anti-NP IgG1 serum titers were indistinguishable comparing *Cpa3*$^{+/+}$ and *Cpa3*$^{Cre/+}$ mice (Figure 5C). Hence, mast cell-deficient mice can mount a normal T cell-dependent antibody response to hapten-carrier including class switch (Figure 5C) and hypermutation (not shown).

Taken together, with the exception of reduced basophils, all tested hematological and immunological parameters did not differ between *Cpa3*$^{+/+}$ and *Cpa3*$^{Cre/+}$ mice. Likewise, the lack of mast cells in *Cpa3*$^{Cre/+}$ mice had no impact on a Th2 cell-dependent antibody response.

Impact of Mast Cell Deficiency and Kit Deficiency on Susceptibility to Antibody-Induced Arthritis in the K/BxN Model

The concept that mast cells contribute to autoimmunity has gained considerable attention (reviewed in Benoist and Mathis, 2002; Sayed et al., 2008). This was propelled by the inability to induce the K/BxN serum transfer arthritis in mast cell-deficient *Kit*$^{W/Wv}$ mice and in mast cell-deficient Kit ligand (Kitl)-mutated *Kitl*$^{Sl/Sld}$ mice (Lee et al., 2002). In the K/BxN autoimmune arthritis model (Kouskoff et al., 1996), K/BxN mice spontaneously produce IgG antibodies that react with the ubiquitous cytoplasmic enzyme glucose-6-phosphate isomerase (GPI). Intraperitoneal (i.p.) injection of K/BxN serum passively transfers the arthritis to naive recipient mice with rapid onset within days and severe progression (Korganow et al., 1999). Immune complex depositions in the joints initiate and promote inflammation and joint destruction (reviewed in Benoist and Mathis, 2002).

To analyze the susceptibility of *Kit*-proficient mice lacking mast cells to serum transfer arthritis, we challenged *Cpa3*$^{Cre/+}$ mice and their wild-type *Cpa3*$^{+/+}$ controls (both C57BL/6), as well as *Kit*$^{W/Wv}$ mice (WB × C57BL/6 F1) by i.p. injections with K/BxN mouse serum (Figure 6). *Cpa3*$^{+/+}$ and *Cpa3*$^{Cre/+}$ mice were littermates kept together in common cages, and the scoring was done on genotype-blind animals. This routine procedure, which avoids experimental bias, has not been possible before because WB × C57BL/6 F1 *Kit*$^{W/Wv}$ mice are white whereas control WB × C57BL/6 F1 *Kit*$^{+/+}$ mice are black. *Kit*$^{W/Wv}$ mice were bred from heterozygous parents in the same mouse room as the *Cpa3*$^{+/+}$ and *Cpa3*$^{Cre/+}$ mice.

Each day after the first injection of the K/BxN serum, hind limb ankle thickness and the clinical score were recorded. In the first experiment, we compared *Cpa3*$^{+/+}$, *Cpa3*$^{Cre/+}$, and *Kit*$^{W/Wv}$ mice (Figure 6A). Wild-type mice showed the reported rapid onset and severe progression of disease. Both ankle joint swelling and clinical score peaked around day 12 and improved thereafter but did not fully resolve. *Kit*$^{W/Wv}$ mice were protected from the disease, except for very mild and transient symptoms (Lee et al., 2002). In contrast to *Kit*$^{W/Wv}$ mice, *Cpa3*$^{Cre/+}$ mice were clearly susceptible. Hence, *Kit*$^{W/Wv}$ mice were protected whereas both *Cpa3*$^{+/+}$ and *Cpa3*$^{Cre/+}$ mice developed severe arthritis. This finding was confirmed in a second experiment comparing *Cpa3*$^{+/+}$ and *Cpa3*$^{Cre/+}$ mice (Figure 6B). Data in Figures 6A and 6B were subjected to a two-way ANOVA considering time and genotypes to evaluate differences in response curves. No significant differences between *Cpa3*$^{+/+}$ and *Cpa3*$^{Cre/+}$ genotypes were observed (p values > 0.05 for clinical scores and for ankle thickness in Figures 6A and 6B).

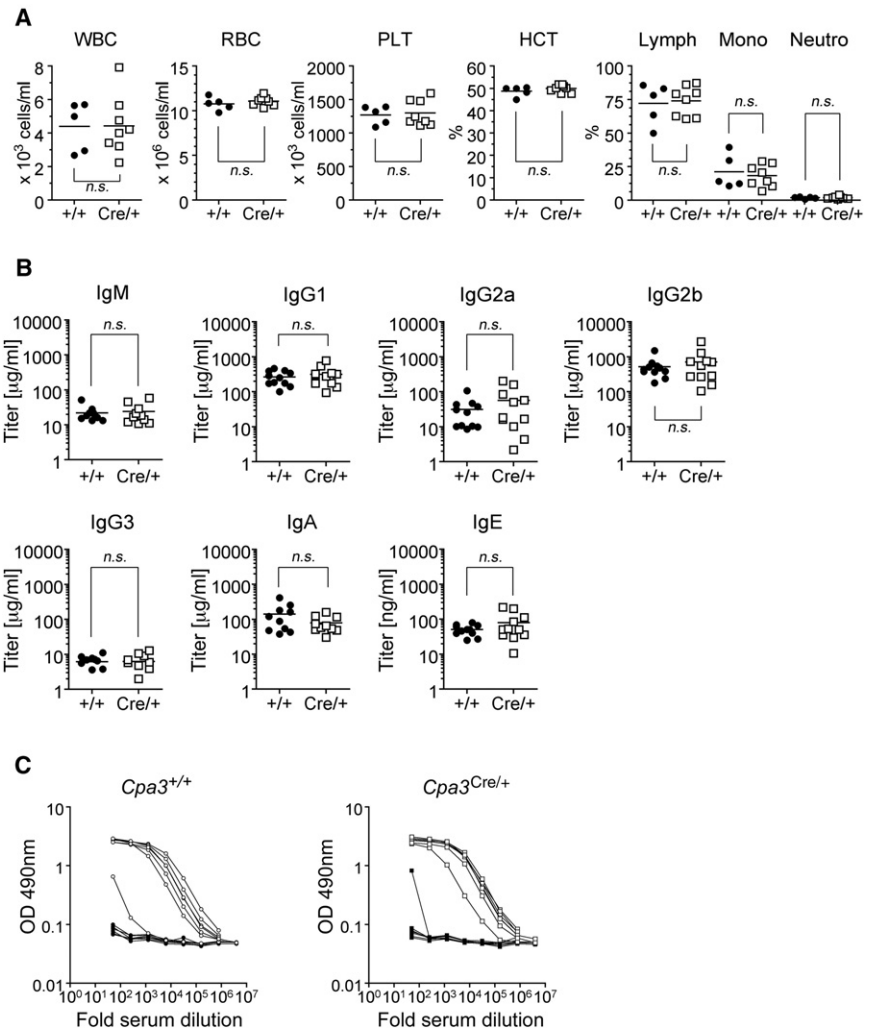

Figure 5. Hematological and Immunological Parameters, Including a Th2 Cell-Dependent Antibody Response in the Absence of Mast Cells

(A) Peripheral blood from *Cpa3*$^{+/+}$ (closed circle) and *Cpa3*$^{Cre/+}$ (open square) mice was analyzed for total cell numbers of white blood cells (WBC), red blood cells (RBC), platelets (PLT), hematocrit (HCT), and percentages of lymphocytes (Lymph), monocytes (Mono), and neutrophils (Neutro). Detailed data on hematopoetic populations are shown in Figure S5.

(B) Serum immunoglobulin concentrations of IgM, IgG1, IgG2a, IgG2b, IgG3, IgA, and IgE were determined for nonimmunized *Cpa3*$^{+/+}$ (closed circle) and *Cpa3*$^{Cre/+}$ (open square) mice. In (A) and (B), each symbol represents an individual mouse. None of the values differed significantly between *Cpa3*$^{+/+}$ and *Cpa3*$^{Cre/+}$ mice (all p values > 0.05 for *Cpa3*$^{+/+}$ versus *Cpa3*$^{Cre/+}$ mice).

(C) Anti-NP IgG1 titers were measured in preimmune (closed circle) and immunized (open circle) *Cpa3*$^{+/+}$ (n = 7) and in preimmune (closed square) and immunized (open square) *Cpa3*$^{Cre/+}$ (n = 7) mice 14 days after immunization with NP-chicken gamma globulin. Serum dilutions are plotted versus optical density (OD) readings. Each line represents an individual mouse.

These conclusions were corroborated by histopathological evaluations of ankle joints from K/BxN serum-injected *Cpa3*$^{+/+}$ mice, which showed massive leukocyte infiltrations, erosion of the cartilage, and destruction of the functional joint. These pathological alterations were also present in ankle joints of *Cpa3*$^{Cre/+}$ but not of *Kit*$^{W/Wv}$ or PBS-injected *Cpa3*$^{+/+}$ mice (Figure 6C).

As a measure of disease progression and severity, we next compared arthritis-associated changes in gene expression. In this third independent experiment, ankle joints were collected from naive mice and from mice 3 and 7 days after the first injection of K/BxN serum. Global gene expression analysis revealed several distinct patterns: (1) genes that are upregulated toward day 7, (2) genes that are upregulated beginning on day 3 and continuing through day 7, (3) genes that are, regardless of the time point, present in *Cpa3*$^{+/+}$ but absent in *Cpa3*$^{Cre/+}$ mice, and (4) genes that are downregulated toward day 7. Patterns 1, 2, and 4 are reminiscent of an earlier report (Jacobs et al., 2010) and were comparable between *Cpa3*$^{+/+}$ and *Cpa3*$^{Cre/+}$ mice (Figure 6D). This is further support for the comparable clinical course and histopathological data obtained in these two strains (Figures 6A–6C). Pattern 3 showed that the mast cell products *Cma2*, *Cpa3*, *Mcpt4*, and *Mcpt5* were not present in the joints of *Cpa3*$^{Cre/+}$ mice before or during the joint inflammation. In further search for mast cell products, we also analyzed joints by RT-PCR for expression of *Mcpt4*, *Mcpt5, Mcpt6,* and *Fcer1a* (Figure 6E). As a control for induction of arthritis, we included inflammatory markers *Saa3* and *Mmp3*, which are upregulated in arthritic joints in this model (Jacobs et al., 2010). All of these mast cell genes were expressed in joints of *Cpa3*$^{+/+}$ mice and did not increase with inflammation. None of the mast cell products examined in the mRNA array or in the RT-PCR were found in naive or inflamed joints of *Cpa3*$^{Cre/+}$ mice (Figures 6D and 6E). In brief, K/BxN antibody arthritis did not induce mast cell products in *Cpa3*$^{Cre/+}$ joints at any time point analyzed, and mast cell products, although present in wild-type mice, were not upregulated in the course of the disease.

Collectively, disease progression and severity were evaluated based on joint thickness, clinical scores, histopathology, and arthritis-associated changes in gene expression. The results showed that mast cell-deficient *Cpa3*$^{Cre/+}$ mice and wild-type *Cpa3*$^{+/+}$ controls were comparably susceptible in the K/BxN autoimmune arthritis model, whereas *Kit*$^{W/Wv}$ mice were largely protected. The full susceptibility of *Cpa3*$^{Cre/+}$ mice makes the idea of a crucial role for mast cells in this immune complex model of arthritis unlikely.

Cpa3$^{Cre/+}$ and *Kit*$^{W/Wv}$ Mice Are Susceptible to Experimental Autoimmune Encephalomyelitis

It has been reported that mast cells are important in experimental autoimmune encephalomyelitis (EAE), which serves as a model

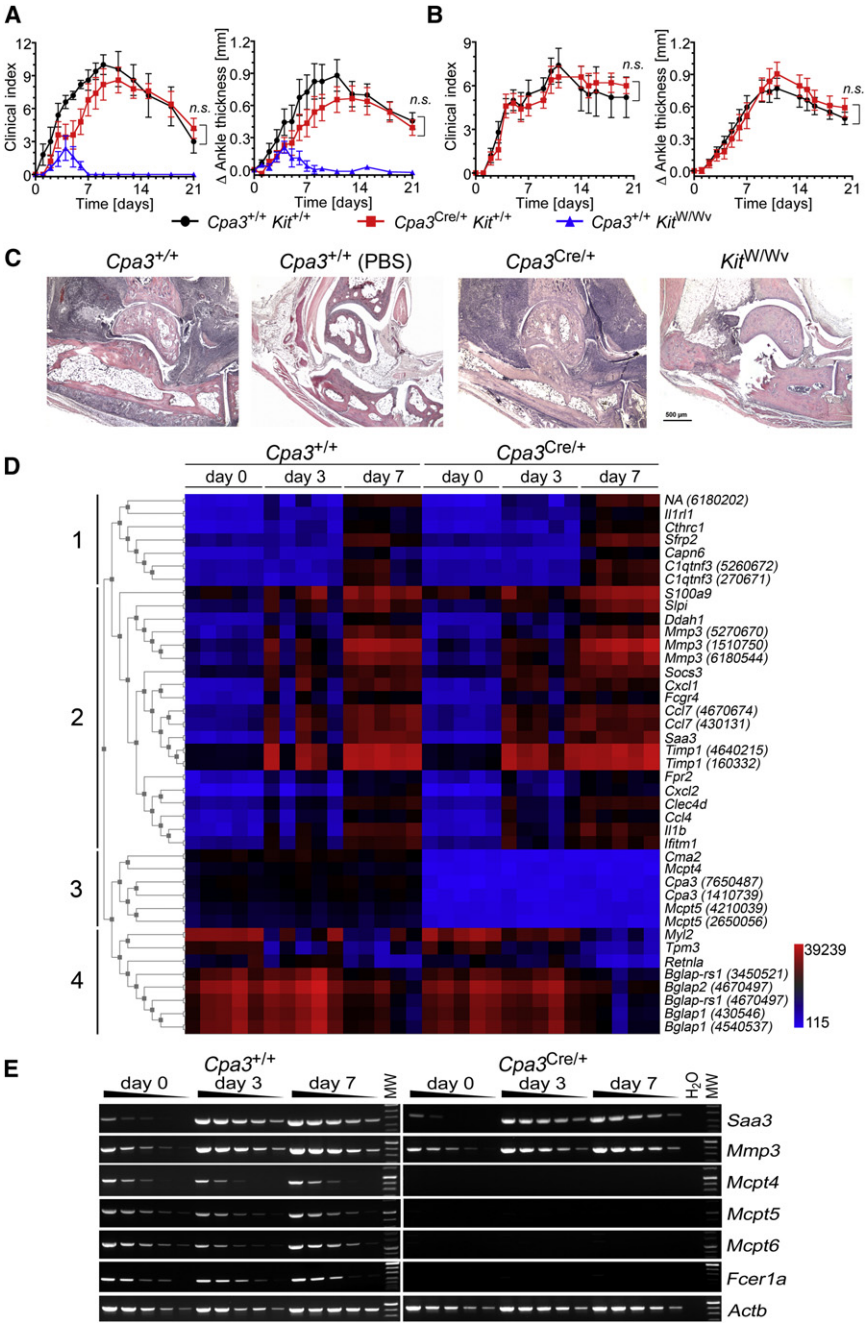

Figure 6. Antibody-Induced Arthritis Independent of Mast Cells but Dependent on Kit

(A and B) Kinetics and severity of K/BxN serum transfer arthritis in *Cpa3*$^{+/+}$ (closed black circle), *Cpa3*$^{Cre/+}$ (closed red square), and *Kit*$^{W/Wv}$ (closed blue triangle) mice. In experiment 1 (A), *Cpa3*$^{+/+}$, *Cpa3*$^{Cre/+}$, and *Kit*$^{W/Wv}$ mice (n = 5 for each genotype) were compared, and in experiment 2 (B), *Cpa3*$^{+/+}$ and *Cpa3*$^{Cre/+}$ mice (n = 5 for each genotype) were analyzed side-by-side. Clinical scoring (Clinical index) was done as described in Experimental Procedures, and the data are plotted as mean daily clinical score ± SEM for all animals per group. Ankle thickening is expressed as increase in thickness (Δ) compared to the baseline ankle thickness of each paw and is shown as the mean ± SEM of both hind limbs. No significant differences between *Cpa3*$^{+/+}$ and *Cpa3*$^{Cre/+}$ genotypes were observed for clinical scores (A, p = 0.11; B, p = 0.95) and for ankle thickness (A, p = 0.38; B, p = 0.81).

(C) Histopathological analysis of ankle joints. 10 days after injection of K/BxN serum (*Cpa3*$^{+/+}$, *Cpa3*$^{Cre/+}$, and *Kit*$^{W/Wv}$) or saline (*Cpa3*$^{+/+}$ PBS), joints were stained by hematoxylin and eosin (H&E). The affected *Cpa3*$^{+/+}$ joint shows very severe destructive rheumatoid-like osteoarthritis with tendovaginitis and adjacent granuloma formation. It is further characterized by active, granulocytic inflammation giving rise to granulocytic exudates into tendon sheaths and appearance of metaplastic ossifocation within the inflammatory pannus. Similarly, the *Cpa3*$^{Cre/+}$ joint suffers from severe proliferative and granulomatous rheumatoid-like arthitis and tendovaginitis with osteoarthrosis. In contrast, the joints from K/BxN serum-injected *Kit*$^{W/Wv}$ mice and the non-injected *Cpa3*$^{+/+}$ control present as normal joints without any pathology.

(D) Changes in gene expression in response to K/BxN serum arthritis. Global mRNA expression was analyzed in ankle joints from naive mice (day 0) and from mice 3 and 7 days after the first injection of K/BxN serum. For each genotype and time point, a total of five joints from 3–4 individual mice were analyzed. Four distinct patterns of changes in gene expression are indicated on the left (1–4) (see Results). Pattern 3 shows lack of mast cell products in *Cpa3*$^{Cre/+}$ mice at all time points.

(E) RT-PCR analysis on 4-fold dilutions of the cDNAs (joints as described in D) for expression of mast cell products *Mcpt4*, *Mcpt5, Mcpt6,* and *Fcer1a*, of inflammatory markers *Saa3* and *Mmp3*, and of *Actb* as positive control.

for human multiple sclerosis (MS). Mast cell numbers and their distribution correlate with the development of MS or EAE (reviewed in Sayed et al., 2008), and *Kit*$^{W/Wv}$ and *Kit*$^{W\text{-}sh/W\text{-}sh}$ mice were reported to be more resistant than *Kit*$^{+/+}$ mice to myelin oligodendrocyte glycoprotein $(MOG)_{35–55}$ (termed MOG) peptide-induced EAE (Secor et al., 2000; Stelekati et al., 2009).

Cpa3$^{+/+}$, *Cpa3*$^{Cre/+}$, and *Kit*$^{W/Wv}$ mice were subjected to MOG-induced EAE (Figures 7 and S6; Mendel et al., 1995). We monitored onset of disease, incidence of diseased mice, numbers of moribund mice, and the maximal score (see Experimental Procedures for the scoring system) over the observation period. *Cpa3*$^{+/+}$ and *Cpa3*$^{Cre/+}$ mice were mixed littermates that were scored without prior knowledge of their *Cpa3* genotype.

We compared *Cpa3*$^{+/+}$, *Cpa3*$^{Cre/+}$, and *Kit*$^{W/Wv}$ mice in three independent EAE experiments (Figures 7 and S6). Analysis of *Cpa3*$^{+/+}$ (n = 19), *Cpa3*$^{Cre/+}$ (n = 19), and *Kit*$^{W/Wv}$ (n = 11) mice revealed comparable days of onset of disease (mean 10.6 ± 1.1 [one standard deviation; SD] for *Cpa3*$^{+/+}$; 11.0 ± 1.6 for *Cpa3*$^{Cre/+}$; 11.1 ± 0.9 for *Kit*$^{W/Wv}$) (Figures 7A–7D and S6). The incidence was 100% in all three strains and the maximal score

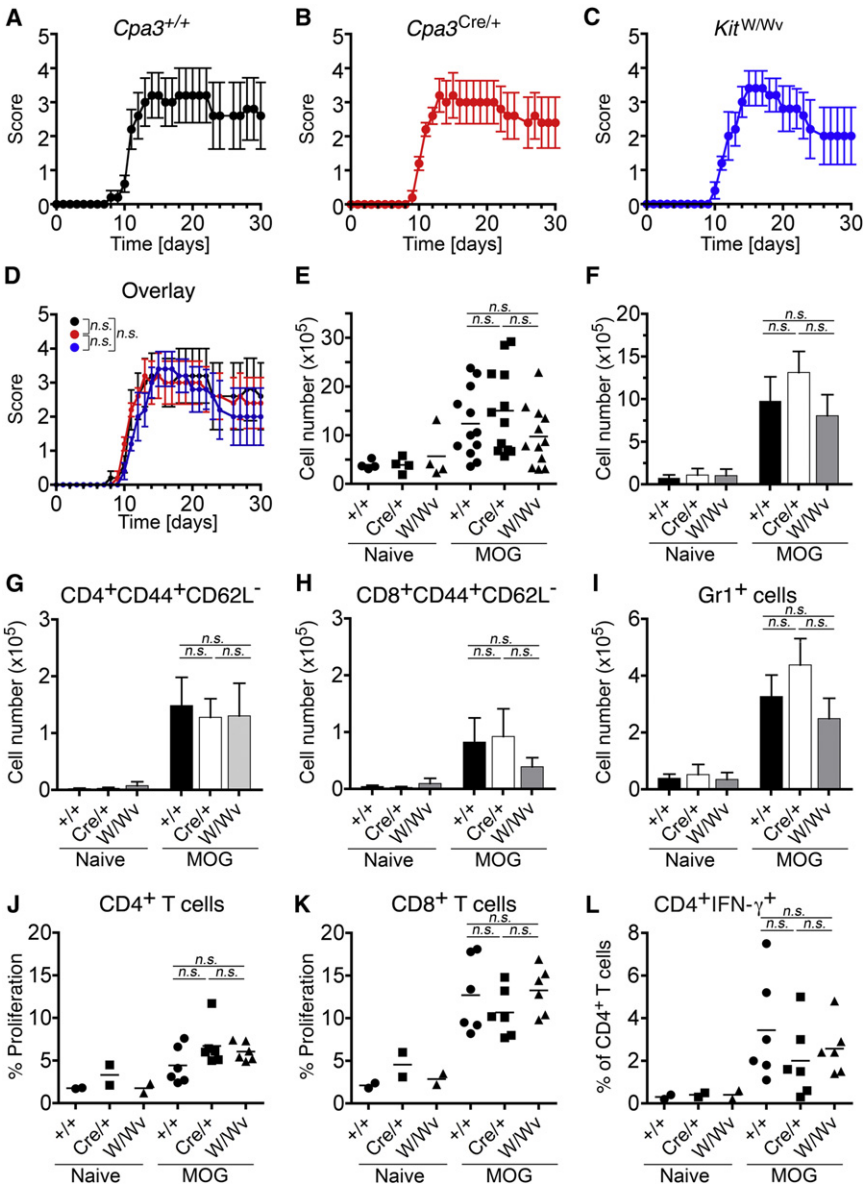

Figure 7. Experimental Autoimmune Encephalomyelitis Independent of Mast Cells and Independent of Kit

(A–D) Kinetics and severity of MOG-induced EAE in *Cpa3*$^{+/+}$ (A), *Cpa3*$^{Cre/+}$ (B), and *Kit*$^{W/Wv}$ (C) mice. Overlay (D) shows direct comparison of *Cpa3*$^{+/+}$ (black circle), *Cpa3*$^{Cre/+}$ (red circle), and *Kit*$^{W/Wv}$ (blue circle) mice. Shown are the mean ± SEM of the clinical score with n = 5 for each genotype. Based on a two-way ANOVA considering time and genotypes, no significant differences were found in (D) (p = 0.92 for *Cpa3*$^{+/+}$ versus *Cpa3*$^{Cre/+}$, p = 0.69 for *Cpa3*$^{+/+}$ versus *Kit*$^{W/Wv}$, and p = 0.74 for *Cpa3*$^{Cre/+}$ versus *Kit*$^{W/Wv}$) (see also Figure S6).

(E) Total mononuclear cells in the central nervous system (CNS). Naive (n = 4) and MOG-immunized (n = 12) mice were compared in a total of four independent experiments.

(F–H) Numbers of lymphocytes (F), activated (CD44$^+$CD62L$^-$) CD4$^+$ (G), and CD8$^+$ (H) T cells in the CNS of naive and MOG-immunized mice of the indicated genotypes.

(I) Numbers of Gr1$^+$ granulocytes in the CNS of naive and MOG-immunized mice of the indicated genotypes.

(J and K) In vitro proliferative response of splenic CD4$^+$ (J) and CD8$^+$ (K) T cells from naive and MOG-immunized mice of the indicated genotypes.

(L) Splenic CD4$^+$ T cells as described in (J) were stimulated overnight with MOG peptide and the percentages of IFN-γ$^+$CD4$^+$ T cells were determined by flow cytometry after intracellular cytokine staining.

Analyses in (E)–(L) were done 11 days after immunization. Data in (E) summarize four independent experiments. In (F)–(L), naive (n = 2) and MOG-immunized (n = 6) mice were compared in two independent experiments. In (E)–(L), the indicated genotypes of all MOG-immunized mice were statistically compared and none were found significantly different (all p values > 0.05).

was 3.7 ± 1.0 for *Cpa3*$^{+/+}$, 3.3 ± 0.9 for *Cpa3*$^{Cre/+}$, and 3.8 ± 1.4 for *Kit*$^{W/Wv}$ mice. Finally, numbers of moribund mice were 4/19 (21%) for *Cpa3*$^{+/+}$, 3/19 (16%) for *Cpa3*$^{Cre/+}$, and 5/11 (46%) for *Kit*$^{W/Wv}$ mice (Figure S6). Based on a two-way ANOVA considering time and genotypes, no significant differences were found between any of the strains (Figures 7D, S6A, and S6B: p values > 0.05 for all comparisons of *Cpa3*$^{+/+}$ versus *Cpa3*$^{Cre/+}$, *Cpa3*$^{+/+}$ versus *Kit*$^{W/Wv}$, and *Cpa3*$^{Cre/+}$ versus *Kit*$^{W/Wv}$ mice). Hence, all three strains were indistinguishable for the onset of disease, the mean maximal score, and the incidence.

In further search for genotype-related differences, we analyzed the extent of leukocyte infiltration into the central nervous system (CNS) and the associated effector T cell response in MOG-immunized mice (Figures 7E–7L). These analyses were done on day 11 postimmunization, i.e., at the beginning of the onset of clinical signs of disease. Consistent with neurological symptoms, absolute numbers of leukocytes retrieved from the CNS strongly increased in all three strains compared to nonimmunized mice (Figure 7E). *Cpa3*$^{+/+}$, *Cpa3*$^{Cre/+}$, and *Kit*$^{W/Wv}$ mice showed a comparable increase in CD45^{hi} lymphocytes (Figure 7F), which included both CD4$^+$ and CD8$^+$ T cells with an activated-memory phenotype (CD44$^+$CD62L$^-$) (Figures 7G and 7H). All three strains showed strong influx of Gr1$^+$ neutrophils to the CNS at day 11 postimmunization (Figure 7I), whereas the relative fraction of F4/80$^+$ cells (probably mostly microglia) declined relative to neutrophils (not shown). MOG immunization led to an in vivo expansion of MOG-reactive T cells as shown by proliferation of splenic CD4$^+$ and CD8$^+$ T cells (Figures 7J and 7K) and IFN-γ production by CD4$^+$ T cells upon restimulation with MOG peptide in vitro (Figure 7L).

In summary, these experiments demonstrated that normal *Cpa3*$^{+/+}$ and mast cell-deficient *Cpa3*$^{Cre/+}$ mice were indistinguishably susceptible to the development of MOG-induced EAE. Unexpectedly, *Kit*$^{W/Wv}$ mice were equally vulnerable

compared to $Cpa3^{+/+}$ or $Cpa3^{Cre/+}$ mice, suggesting that neither mast cell deficiency nor Kit deficiency affect the clinical or immunological manifestation of MOG-induced EAE.

DISCUSSION

Since the discovery that mast cell development depends on Kit (Kitamura et al., 1978), *Kit* mutants have been used to examine in vivo mast cell functions. $Kit^{W/Wv}$ mice not only lack mast cells but suffer from additional defects, notably anemia, neutropenia, and lack of subsets of intraepithelial lymphocytes. In addition, they show impairments in lymphocyte development, gut motility, and pain sensation. $Kit^{W\text{-}sh/W\text{-}sh}$ mice display a milder spectrum of abnormalities and, given their fertility and their C57BL/6 background, seem a better model than $Kit^{W/Wv}$ mice (Grimbaldeston et al., 2005). However, the genetic inversion in $Kit^{W\text{-}sh/W\text{-}sh}$ mice is associated with further hematopoietic abnormalities, including splenomegaly with expanded myeloid and megakaryocyte populations, neutrophilia (in contrast to the neutropenia of $Kit^{W/Wv}$ mice), and thrombocytosis (Nigrovic et al., 2008; Zhou et al., 2007).

To distinguish *Kit* deficiency from mast cell deficiency, mast cell-reconstitution of *Kit* mutants became an experimental cornerstone for studies of in vivo mast cell functions (Tsai et al., 2005). A definitive separation of *Kit* deficiency from mast cell deficiency may be aided by *Kit* mutation-independent mast cell-deficient mice. Here, we have presented a mouse mutant that satisfies these criteria. Mast cell deficiency was demonstrated by several independent approaches, i.e., flow cytometry, histology, mRNA array analyses, and after challenges with intestinal parasites, during acute arthritis, and in chronic PMA-induced dermatitis. By none of these criteria did Cre-Master mice harbor mast cells or their products. Functionally, Cre-Master mice did not respond when challenged by anaphylaxis, and this defect was rescued by reintroduction of mast cells.

In the light of the widespread use of Cre, it was surprising to find full mast cell ablation in $Cpa3^{Cre/+}$ mice. What could be the mechanism of mast cell ablation? Based on a $Cpa3^{humanCD4}$ gene-targeted reporter mouse, in which *Cpa3* expression can be visualized by cell surface expression of human CD4 (unpublished), the *Cpa3* locus is weakly expressed in several hematopoietic progenitors, including splenic basophil and mast cell progenitors (BMCPs) (Arinobu et al., 2005), and in splenic basophils. Consistent with weak expression of the *Cpa3* locus, splenic BMCPs were present in normal numbers in $Cpa3^{Cre/+}$ mice. In contrast, *Cpa3* expression in mast cells is very strong, i.e., ~14-fold higher than in BMCPs. This progressive increase of Cpa3 expression with development was paralleled by a concomitant loss of cells (not shown). The partial reduction in basophils is probably caused by a similar mechanism because *Cpa3* is also expressed in this cell type. In $Cpa3^{Cre/+}$ mice, basophils in the spleen were reduced to ~40%. This reduction should be considered when immunological functions are assessed in this strain. Markedly reduced numbers of basophils in peripheral blood (Mancardi et al., 2011) and spleen (this paper) in $Kit^{W/Wv}$ mice suggest that a combined effect on these developmentally related lineages may not be unique for $Cpa3^{Cre/+}$ mice.

$Cpa3^{Cre/+}$ BMMCs carried genomic deletions and a pseudotrisomy that is supportive of a genotoxic mechanism of mast cell ablation. The mast cell rescue showed that this mechanism is, at least partly, Trp53 dependent. The lethal effect of $Cpa3^{Cre}$ expression on mast cells is reminiscent of a selective ablation of basophils in *Mcpt8-Cre* BAC transgenic mice (Ohnmacht et al., 2010), suggesting that both mast cells and basophils are sensitive to Cre overexpression. It remains to be determined whether these two lineages are more sensitive to genotoxicity of Cre than other cell types. Finally, global analysis of the expression of chemokines, cytokines, Fc receptors, and adhesion molecules revealed that the mechanism of mast cell ablation in Cre-Master mice does not cause any apparent signs of inflammation or ongoing immune responses.

Recently, two other mouse lines have been generated with the aim of expressing Cre in mast cells. In contrast to $Cpa3^{Cre/+}$ mice, in which Cre was inserted via gene targeting, *Mcpt5-Cre* (Scholten et al., 2008) and alpha-chymase promoter-Cre (*Chm:Cre*) (Müsch et al., 2008) strains are transgenic lines. All three strains have distinct patterns of Cre expression. Whereas $Cpa3^{Cre}$ is expressed in all mast cell subtypes, including the progenitor, *Mcpt5-Cre* mice display expression in connective tissues (peritoneal cavity and skin) while *Chm:Cre* mice show a mucosal expression pattern (lung and colon but not peritoneal cavity). A further difference is the constitutive mast cell deletion by the $Cpa3^{Cre}$ allele, which does not occur in *Mcpt5-Cre* and *Chm:Cre* mice. Hence, $Cpa3^{Cre/+}$ mice represent a constitutive mast cell deficiency model, whereas *Mcpt5-Cre* and *Chm:Cre* allow deletion of floxed genes in distinct mast cell populations.

Mast cells have widely been considered enigmatic cells whose physiological functions and medical importance beyond the undesired allergy might still await discovery (Galli, 1993; Kaliner, 1979). Among the recently suggested functions for mast cells were protective roles ("sentinels of pathogens") not only against parasites but also against bacteria and viruses (reviewed in Abraham and St John, 2010). In addition, several authors have recently emphasized immunomodulatory mechanisms in which both innate and adaptive immune responses are guided early on by mast cells and their products (Galli et al., 2005, 2008; Abraham and St John, 2010; Frossi et al., 2010; Dietrich et al., 2010). In this context belong reports that mast cells are key cellular elements in autoimmune diseases (reviewed in Benoist and Mathis, 2002; Sayed et al., 2008; de Vries and Noelle, 2010). As a new entry point for a systematic analysis of the possible roles of mast cells in autoimmunity, we have focused our experiments by using Cre-Master mice on two prominent models of autoimmune diseases, autoantibody-driven arthritis and EAE. In the case of the K/BxN arthritis, we confirmed an earlier finding that $Kit^{W/Wv}$ mice are overall resistant while wild-type mice are susceptible (Lee et al., 2002). However, our result that $Kit^{+/+}$ mice lacking mast cells ($Cpa3^{Cre/+}$) are fully susceptible to the disease makes roles for mast cells in this particular autoimmune pathology unlikely. The discrepancy between susceptible $Kit^{+/+}$ mice lacking mast cells ($Cpa3^{Cre/+}$) and resistant $Kit^{W/Wv}$ mice suggests an important role for Kit in this model. Transfer of mast cells rendered $Kit^{W/Wv}$ mice susceptible to the K/BxN serum transfer arthritis (Lee et al., 2002). The fact that we found no evidence for a role of mast cells in the context of a normal immune system raises the possibility that mast cells have a propathogenic effect in the context of *Kit* deficiency. That factors other than mast cells may be crucial has also

been supported in a passive model of arthritis induced by collagen mAbs, which yielded conflicting results comparing $Kit^{W/Wv}$ and $Kit^{W\text{-}sh/W\text{-}sh}$ mice (Zhou et al., 2007).

Data obtained in the EAE model warrant some additional considerations. Based on analysis of pure C57BL/6 mice without mast cells (Cre-Master), we consider a major role for mast cells in MOG-induced EAE induction or progression unlikely. In the literature, there are substantial variations in MOG-induced EAE results in $Kit^{W/Wv}$ mice, their MHC-syngeneic wild-type litter mate controls (WB × C57BL/6 $Kit^{+/+}$), and mast cell-reconstituted $Kit^{W/Wv}$ mice (Bennett et al., 2009; Secor et al., 2000). Although the reasons for these discrepancies may be manifold, e.g., mouse colony conditions, microbiota colonization of mice, or subjective scoring of clinical parameters, our side-by-side analysis of EAE in $Cpa3^{+/+}$, $Cpa3^{Cre/+}$, and $Kit^{W/Wv}$ mice suggests that correlations between the numbers and the distribution of mast cells and EAE pathology do not reflect an active role of mast cells in this disease.

Collectively, we have generated a mouse line lacking mast cells by targeted expression of Cre recombinase from the *Cpa3* locus. These mast cell-deficient mice have a normal immune system but are unable to mount IgE-mediated allergic responses. However, they are fully susceptible to antibody-induced autoimmune arthritis and to experimental autoimmune encephalomyelitis. Although we do not question data obtained in *Kit* mutant mice per se, our data provide an example in which the selective absence of mast cells has different consequences than the combined deficiency of mast cells and Kit. In our view, these discrepancies call for a systematic re-evaluation of immunological functions of mast cells beyond allergy.

EXPERIMENTAL PROCEDURES

Gene Targeting and Mice

Generation of $Cpa3^{Cre}$ gene-targeted mice was done as described in the Supplemental Experimental Procedures. All animal procedures were approved by the local animal committees (Regierungspräsidien Tübingen and Karlsruhe or Kantonales Veterinäramt Zürich) and performed in accordance with the institutional guidelines. $Cpa3^{+/+}$ and $Cpa3^{Cre/+}$ mice were littermates from at least 12 backcrosses to C57BL/6 or the fourth backcross on BALB/c.

Flow Cytometry and Blood Analyses

Antibodies used are listed in the Supplemental Experimental Procedures. Cells were stained for flow cytometry as described (Rodewald et al., 1997) and analyzed on FACS Canto II and LSRFortessa instruments with Diva Software (BD Biosciences). Hemocytometric parameters of tail vein blood were obtained on an automated hemocytometer according to the manufacturer's instructions (ADVIA120; Bayer, Leverkusen, Germany).

Histochemistry

Peritoneal lavage cells were cytospun as described (Feyerabend et al., 2005) and stained by May-Grünwald-Giemsa. Tissue mast cells were stained by toluidine blue as described (Feyerabend et al., 2005) or by chloroacetate esterase (CAE) staining (Supplemental Experimental Procedures).

Skin Inflammation

Phorbol-12-myristate-13-acetate (PMA)-induced skin inflammation was induced and analyzed as described previously (Waskow et al., 2007).

Anaphylaxis

Passive cutaneous anaphylaxis was done as described (Feyerabend et al., 2005). For body temperature measurements in passive systemic anaphylaxis, mice were sensitized intravenously with 20 μg anti-DNP IgE (Sigma), and temperature was monitored rectally after challenge on the next day with 20 μg DNP_{11}-Ova (Biocat). To rescue the defect in anaphylaxis, $Cpa3^{Cre/+}$ mice were transplanted with cultured mast cells, derived as described (Feyerabend et al., 2005), and challenged by IgE and DNP-Ova. For blood pressure analyses, mice were sensitized with 50 μg anti-DNP IgE and challenged on the next day with 500 μg $DNP_{30\text{-}40}$-HSA (Sigma). Blood pressure measurements were done on anesthetized mice as described in Supplemental Experimental Procedures.

Serum Immunoglobulins and Anti-NP Immune Response

Steady-state serum immunoglobuline isotypes were quantified with an anti-kappa light chain capture antibody, mouse immunoglobuline standards, and horseradish peroxidase-linked isotype-specific detection antibodies (listed in the Supplemental Experimental Procedures). Tetramethylbenzidine substrate conversion was read at 450 nm on a SpectraMax250 spectrometer (MWG Biotech). NP-specific antibodies were measured in the serum 2 weeks after i.p. immunization with 100 μg of 4-hydroxy-3-nitrophenylacetyl-chicken gamma globulin (NP-CGG, Biosearch Technologies) supplemented with 50 μl Adju-Phos 2% Alum (HCl Biosector). NP-BSA-coated plates, an HRP-linked IgG1-specific detection antibody, and o-phenylenediamine dihydrochloride substrate were used for ELISA. OD values were read at 490 nm.

RNA Expression Analyses

RNA extraction and microarray expression analyses were performed at the DKFZ genomics and proteomics core facility and were done as described in Supplemental Experimental Procedures. Samples were hybridized to the MouseWG-6 v2.0 BeadChip (Illumina). Heat maps of selected genes (Figure 1) were assembled with the Gene Pattern software package (Broad Institute, MIT). Hierarchical clustering (Figure 6) was performed with Chipster CSC v1.4.7. Differentially expressed genes were filtered by standard deviation (3 SDs = 99.7%), subjected to a several groups test (empirical Bayes method with Benjamini-Yakutieri test), and hierarchically clustered by Pearson correlation. Preparation of cDNAs and primer sequences for RT-PCRs are described in the Supplemental Experimental Procedures.

Parasite Infection

Mice were infected subcutaneously with 400 live L3 parasites (Supplemental Experimental Procedures). At day 10 or 14 after infection, the upper portion of the jejunum was processed for histology or for RT-PCR and serum was taken for Mcpt1-specific ELISA (Supplemental Experimental Procedures).

K/BxN Serum Arthritis

12-week-old mice were injected i.p. with 150 μl of pooled arthritogenic K/BxN serum (Korganow et al., 1999) on experimental days 0 and 2. Mice were evaluated daily for arthritis severity. Each paw was evaluated and scored individually with the following scoring system: 0, no evidence of erythema and swelling; 1, erythema and mild swelling; 2, erythema and pronounced edematous swelling; 3, ankylosis of the limb. Additionally, ankle thickness of the hind limbs was measured with a precision caliber (Käfer; dial thickness gauge). For histopathology, ankles were taken on day 10 after the first K/BxN serum injection, fixed with paraformaldehyde, decalcified in Kristensen's solution, embedded in paraffin, and cut in 5 μm sections, and mid-sagittal ankle sections were stained with hematoxylin and eosin (H&E).

EAE

EAE was induced in mice at 13–15 weeks of age as described in Supplemental Experimental Procedures. Individual animals were monitored daily for clinical signs of disease and the disease severity was scored as follows: 0, no signs of disease; 1, limp tail or hind limb weakness; 2, limp tail and hind limb weakness; 3, partial hind limb paralysis; 4, complete hind limb paralysis; 5, moribund or dead. Quantification of CNS-infiltrating mononuclear cells, $MOG_{35\text{-}55}$ peptide restimulation, intracellular cytokine staining, and proliferation are stated in Supplemental Experimental Procedures.

Statistical Analyses

Statistical analyses in Figures 1, 2, 3, 4, 5, and 7E–7L was performed with Prism 4 (GraphPad Software) with the unpaired t test except for Figures 1E and 4D, which were analyzed by one-sample t test. p values are given in the

figures, and $p > 0.05$ was considered nonsignificant (n.s.). A two-way ANOVA for longitudinal data was used to evaluate the differences in response curves of *Cpa3*$^{+/+}$ and *Cpa3*$^{Cre/+}$ mice in Figures 6A, 6B, 7, S6A, and S6B. All computations were performed with the statistical software environment R, version 2.12.2. Values for $p > 0.05$ were considered nonsignificant.

ACCESSION NUMBERS

Data are available in the EMBL-EBI database (http://www.ebi.ac.uk/arrayexpress) under accession numbers E-MTAB-838 and E-MTAB-844.

SUPPLEMENTAL INFORMATION

Supplemental Information includes Supplemental Experimental Procedures and six figures and can be found with this article online at doi:10.1016/j.immuni.2011.09.015.

ACKNOWLEDGMENTS

We thank C. Blum for blastocyst injections; C. Haber, N. Maltry, and S. Schäfer for technical assistance; S. Henze, T. Schmidt, and O. Heil (DKFZ Microarray Core Facility) for mRNA analyses; A. Benner (DKFZ Biostatistics) for statistical analyses; M. Feuerer and M. Teichert for heat maps; K. Greulich-Bode for karyotype analysis; M. Reth for discussions on genotoxity; M. Gurish for advice on progenitor isolation; A. Roers for sharing unpublished data; and V. Martins and S. Schlenner for comments on the manuscript. This work was supported by the ERC (Advanced Grant 233074), DFG (754-2-3), and SFB 938-project L to H.-R.R., a grant for A.W. from the Medical Faculty Ulm, awarded to T.B.F., ETH 0-20400-07 to M.K., and R01 AR055271 to C.B. and D.M. T.B.F. and H.-R.R. filed a patent on Cre-driven mast cell eradication.

Received: November 19, 2010
Revised: January 28, 2011
Accepted: September 21, 2011
Published online: November 17, 2011

REFERENCES

Abraham, S.N., and St John, A.L. (2010). Mast cell-orchestrated immunity to pathogens. Nat. Rev. Immunol. *10*, 440–452.

Albuszies, G., Radermacher, P., Vogt, J., Wachter, U., Weber, S., Schoaff, M., Georgieff, M., and Barth, E. (2005). Effect of increased cardiac output on hepatic and intestinal microcirculatory blood flow, oxygenation, and metabolism in hyperdynamic murine septic shock. Crit. Care Med. *33*, 2332–2338.

Aoki, H., Yamada, Y., Hara, A., and Kunisada, T. (2009). Two distinct types of mouse melanocyte: differential signaling requirement for the maintenance of non-cutaneous and dermal versus epidermal melanocytes. Development *136*, 2511–2521.

Arinobu, Y., Iwasaki, H., Gurish, M.F., Mizuno, S.I., Shigematsu, H., Ozawa, H., Tenen, D.G., Austen, K.F., and Akashi, K. (2005). Developmental checkpoints of the basophil/mast cell lineages in adult murine hematopoiesis. Proc. Natl. Acad. Sci. USA *102*, 18105–18110.

Bennett, J.L., Blanchet, M.R., Zhao, L., Zbytnuik, L., Antignano, F., Gold, M., Kubes, P., and McNagny, K.M. (2009). Bone marrow-derived mast cells accumulate in the central nervous system during inflammation but are dispensable for experimental autoimmune encephalomyelitis pathogenesis. J. Immunol. *182*, 5507–5514.

Benoist, C., and Mathis, D. (2002). Mast cells in autoimmune disease. Nature *420*, 875–878.

Berrozpe, G., Timokhina, I., Yukl, S., Tajima, Y., Ono, M., Zelenetz, A.D., and Besmer, P. (1999). The W(sh), W(57), and Ph Kit expression mutations define tissue-specific control elements located between -23 and -154 kb upstream of Kit. Blood *94*, 2658–2666.

Besmer, P., Manova, K., Duttlinger, R., Huang, E.J., Packer, A., Gyssler, C., and Bachvarova, R.F. (1993). The kit-ligand (steel factor) and its receptor c-kit/W: pleiotropic roles in gametogenesis and melanogenesis. Dev. Suppl. 125–137.

Broudy, V.C. (1997). Stem cell factor and hematopoiesis. Blood *90*, 1345–1364.

de Vries, V.C., and Noelle, R.J. (2010). Mast cell mediators in tolerance. Curr. Opin. Immunol. *22*, 643–648.

Di Santo, J.P., and Rodewald, H.R. (1998). In vivo roles of receptor tyrosine kinases and cytokine receptors in early thymocyte development. Curr. Opin. Immunol. *10*, 196–207.

Dietrich, N., Rohde, M., Geffers, R., Kröger, A., Hauser, H., Weiss, S., and Gekara, N.O. (2010). Mast cells elicit proinflammatory but not type I interferon responses upon activation of TLRs by bacteria. Proc. Natl. Acad. Sci. USA *107*, 8748–8753.

Feyerabend, T.B., Hausser, H., Tietz, A., Blum, C., Hellman, L., Straus, A.H., Takahashi, H.K., Morgan, E.S., Dvorak, A.M., Fehling, H.J., and Rodewald, H.R. (2005). Loss of histochemical identity in mast cells lacking carboxypeptidase A. Mol. Cell. Biol. *25*, 6199–6210.

Feyerabend, T.B., Terszowski, G., Tietz, A., Blum, C., Luche, H., Gossler, A., Gale, N.W., Radtke, F., Fehling, H.J., and Rodewald, H.R. (2009). Deletion of Notch1 converts pro-T cells to dendritic cells and promotes thymic B cells by cell-extrinsic and cell-intrinsic mechanisms. Immunity *30*, 67–79.

Fleischman, R.A. (1993). From white spots to stem cells: the role of the Kit receptor in mammalian development. Trends Genet. *9*, 285–290.

Friend, D.S., Ghildyal, N., Austen, K.F., Gurish, M.F., Matsumoto, R., and Stevens, R.L. (1996). Mast cells that reside at different locations in the jejunum of mice infected with *Trichinella spiralis* exhibit sequential changes in their granule ultrastructure and chymase phenotype. J. Cell Biol. *135*, 279–290.

Frossi, B., Gri, G., Tripodo, C., and Pucillo, C. (2010). Exploring a regulatory role for mast cells: 'MCregs'? Trends Immunol. *31*, 97–102.

Galli, S.J. (1993). New concepts about the mast cell. N. Engl. J. Med. *328*, 257–265.

Galli, S.J., Zsebo, K.M., and Geissler, E.N. (1994). The kit ligand, stem cell factor. Adv. Immunol. *55*, 1–96.

Galli, S.J., Kalesnikoff, J., Grimbaldeston, M.A., Piliponsky, A.M., Williams, C.M., and Tsai, M. (2005). Mast cells as "tunable" effector and immunoregulatory cells: recent advances. Annu. Rev. Immunol. *23*, 749–786.

Galli, S.J., Grimbaldeston, M., and Tsai, M. (2008). Immunomodulatory mast cells: negative, as well as positive, regulators of immunity. Nat. Rev. Immunol. *8*, 478–486.

Gordon, J.R., and Galli, S.J. (1990). Phorbol 12-myristate 13-acetate-induced development of functionally active mast cells in W/Wv but not Sl/Sld genetically mast cell-deficient mice. Blood *75*, 1637–1645.

Grimbaldeston, M.A., Chen, C.C., Piliponsky, A.M., Tsai, M., Tam, S.Y., and Galli, S.J. (2005). Mast cell-deficient W-sash c-kit mutant Kit W-sh/W-sh mice as a model for investigating mast cell biology in vivo. Am. J. Pathol. *167*, 835–848.

Higashi, A.Y., Ikawa, T., Muramatsu, M., Economides, A.N., Niwa, A., Okuda, T., Murphy, A.J., Rojas, J., Heike, T., Nakahata, T., et al. (2009). Direct hematological toxicity and illegitimate chromosomal recombination caused by the systemic activation of CreERT2. J. Immunol. *182*, 5633–5640.

Jacobs, J.P., Ortiz-Lopez, A., Campbell, J.J., Gerard, C.J., Mathis, D., and Benoist, C. (2010). Deficiency of CXCR2, but not other chemokine receptors, attenuates autoantibody-mediated arthritis in a murine model. Arthritis Rheum. *62*, 1921–1932.

Kaliner, M.A. (1979). The mast cell—a fascinating riddle. N. Engl. J. Med. *301*, 498–499.

Kitamura, Y., Go, S., and Hatanaka, K. (1978). Decrease of mast cells in W/Wv mice and their increase by bone marrow transplantation. Blood *52*, 447–452.

Korganow, A.S., Ji, H., Mangialaio, S., Duchatelle, V., Pelanda, R., Martin, T., Degott, C., Kikutani, H., Rajewsky, K., Pasquali, J.L., et al. (1999). From systemic T cell self-reactivity to organ-specific autoimmune disease via immunoglobulins. Immunity *10*, 451–461.

Kouskoff, V., Korganow, A.S., Duchatelle, V., Degott, C., Benoist, C., and Mathis, D. (1996). Organ-specific disease provoked by systemic autoimmunity. Cell *87*, 811–822.

Kovanen, P.T. (2009). Mast cells in atherogenesis: actions and reactions. Curr. Atheroscler. Rep. *11*, 214–219.

Lee, D.M., Friend, D.S., Gurish, M.F., Benoist, C., Mathis, D., and Brenner, M.B. (2002). Mast cells: a cellular link between autoantibodies and inflammatory arthritis. Science *297*, 1689–1692.

Liu, J., Divoux, A., Sun, J., Zhang, J., Clément, K., Glickman, J.N., Sukhova, G.K., Wolters, P.J., Du, J., Gorgun, C.Z., et al. (2009). Genetic deficiency and pharmacological stabilization of mast cells reduce diet-induced obesity and diabetes in mice. Nat. Med. *15*, 940–945.

Lu, L.F., Lind, E.F., Gondek, D.C., Bennett, K.A., Gleeson, M.W., Pino-Lagos, K., Scott, Z.A., Coyle, A.J., Reed, J.L., Van Snick, J., et al. (2006). Mast cells are essential intermediaries in regulatory T-cell tolerance. Nature *442*, 997–1002.

Mancardi, D.A., Jönsson, F., Iannascoli, B., Khun, H., Van Rooijen, N., Huerre, M., Daëron, M., and Bruhns, P. (2011). Cutting edge: The murine high-affinity IgG receptor FcγRIV is sufficient for autoantibody-induced arthritis. J. Immunol. *186*, 1899–1903.

Mendel, I., Kerlero de Rosbo, N., and Ben-Nun, A. (1995). A myelin oligodendrocyte glycoprotein peptide induces typical chronic experimental autoimmune encephalomyelitis in H-2b mice: fine specificity and T cell receptor V beta expression of encephalitogenic T cells. Eur. J. Immunol. *25*, 1951–1959.

Metz, M., Piliponsky, A.M., Chen, C.C., Lammel, V., Abrink, M., Pejler, G., Tsai, M., and Galli, S.J. (2006). Mast cells can enhance resistance to snake and honeybee venoms. Science *313*, 526–530.

Müsch, W., Wege, A.K., Männel, D.N., and Hehlgans, T. (2008). Generation and characterization of alpha-chymase-Cre transgenic mice. Genesis *46*, 163–166.

Naiche, L.A., and Papaioannou, V.E. (2007). Cre activity causes widespread apoptosis and lethal anemia during embryonic development. Genesis *45*, 768–775.

Nakano, T., Sonoda, T., Hayashi, C., Yamatodani, A., Kanayama, Y., Yamamura, T., Asai, H., Yonezawa, T., Kitamura, Y., and Galli, S.J. (1985). Fate of bone marrow-derived cultured mast cells after intracutaneous, intraperitoneal, and intravenous transfer into genetically mast cell-deficient W/Wv mice. Evidence that cultured mast cells can give rise to both connective tissue type and mucosal mast cells. J. Exp. Med. *162*, 1025–1043.

Nigrovic, P.A., Gray, D.H., Jones, T., Hallgren, J., Kuo, F.C., Chaletzky, B., Gurish, M., Mathis, D., Benoist, C., and Lee, D.M. (2008). Genetic inversion in mast cell-deficient (Wsh) mice interrupts corin and manifests as hematopoietic and cardiac aberrancy. Am. J. Pathol. *173*, 1693–1701.

Ohnmacht, C., Schwartz, C., Panzer, M., Schiedewitz, I., Naumann, R., and Voehringer, D. (2010). Basophils orchestrate chronic allergic dermatitis and protective immunity against helminths. Immunity *33*, 364–374.

Peters, E.M., Tobin, D.J., Botchkareva, N., Maurer, M., and Paus, R. (2002). Migration of melanoblasts into the developing murine hair follicle is accompanied by transient c-Kit expression. J. Histochem. Cytochem. *50*, 751–766.

Reynolds, D.S., Stevens, R.L., Gurley, D.S., Lane, W.S., Austen, K.F., and Serafin, W.E. (1989). Isolation and molecular cloning of mast cell carboxypeptidase A. A novel member of the carboxypeptidase gene family. J. Biol. Chem. *264*, 20094–20099.

Rodewald, H.-R., Dessing, M., Dvorak, A.M., and Galli, S.J. (1996). Identification of a committed precursor for the mast cell lineage. Science *271*, 818–822.

Rodewald, H.R., Ogawa, M., Haller, C., Waskow, C., and DiSanto, J.P. (1997). Pro-thymocyte expansion by c-kit and the common cytokine receptor gamma chain is essential for repertoire formation. Immunity *6*, 265–272.

Sayed, B.A., Christy, A., Quirion, M.R., and Brown, M.A. (2008). The master switch: the role of mast cells in autoimmunity and tolerance. Annu. Rev. Immunol. *26*, 705–739.

Schmidt-Supprian, M., and Rajewsky, K. (2007). Vagaries of conditional gene targeting. Nat. Immunol. *8*, 665–668.

Schneider, L.A., Schlenner, S.M., Feyerabend, T.B., Wunderlin, M., and Rodewald, H.R. (2007). Molecular mechanism of mast cell mediated innate defense against endothelin and snake venom sarafotoxin. J. Exp. Med. *204*, 2629–2639.

Scholten, J., Hartmann, K., Gerbaulet, A., Krieg, T., Müller, W., Testa, G., and Roers, A. (2008). Mast cell-specific Cre/loxP-mediated recombination in vivo. Transgenic Res. *17*, 307–315.

Secor, V.H., Secor, W.E., Gutekunst, C.A., and Brown, M.A. (2000). Mast cells are essential for early onset and severe disease in a murine model of multiple sclerosis. J. Exp. Med. *191*, 813–822.

Shimshek, D.R., Kim, J., Hübner, M.R., Spergel, D.J., Buchholz, F., Casanova, E., Stewart, A.F., Seeburg, P.H., and Sprengel, R. (2002). Codon-improved Cre recombinase (iCre) expression in the mouse. Genesis *32*, 19–26.

Stelekati, E., Bahri, R., D'Orlando, O., Orinska, Z., Mittrücker, H.W., Langenhaun, R., Glatzel, M., Bollinger, A., Paus, R., and Bulfone-Paus, S. (2009). Mast cell-mediated antigen presentation regulates CD8+ T cell effector functions. Immunity *31*, 665–676.

Tlsty, T.D., and Coussens, L.M. (2006). Tumor stroma and regulation of cancer development. Annu. Rev. Pathol. *1*, 119–150.

Tsai, M., Grimbaldeston, M.A., Yu, M., Tam, S.Y., and Galli, S.J. (2005). Using mast cell knock-in mice to analyze the roles of mast cells in allergic responses in vivo. Chem. Immunol. Allergy *87*, 179–197.

Vousden, K.H., and Lane, D.P. (2007). p53 in health and disease. Nat. Rev. Mol. Cell Biol. *8*, 275–283.

Waskow, C., Bartels, S., Schlenner, S.M., Costa, C., and Rodewald, H.R. (2007). Kit is essential for PMA-inflammation-induced mast-cell accumulation in the skin. Blood *109*, 5363–5370.

Waskow, C., Madan, V., Bartels, S., Costa, C., Blasig, R., and Rodewald, H.R. (2009). Hematopoietic stem cell transplantation without irradiation. Nat. Methods *6*, 267–269.

Zhou, J.S., Xing, W., Friend, D.S., Austen, K.F., and Katz, H.R. (2007). Mast cell deficiency in Kit(W-sh) mice does not impair antibody-mediated arthritis. J. Exp. Med. *204*, 2797–2802.